Excited-State Dynamics and Two-Photon Absorption Cross Sections of Fluorescent Diphenyl-Tin(IV) Derivatives with Schiff Bases: A Comparative Study of the Effect of Chelation from t...

ARTICLE *in* THE JOURNAL OF PHYSICAL CHEMISTRY A · JANUARY 2010

Impact Factor: 2.69 · DOI: 10.1021/jp904784b · Source: PubMed

Excited-State Dynamics and Two-Photon Absorption Cross Sections of Fluorescent Diphenyl-Tin^{IV} Derivatives with Schiff Bases: A Comparative Study of the Effect of Chelation from the Ultrafast to the Steady-State Time Scale

Jimena S. Zugazagoitia,[†] Mauricio Maya,[†] Carlos Damián-Zea,[†] Pedro Navarro,[†] Hiram I. Beltrán,[‡] and Jorge Peon*,[†]

Instituto de Química, Universidad Nacional Autónoma de México, Circuito Exterior, Ciudad Universitaria, 04510 México D.F., México, and Departamento de Ciencias Naturales, UAM-Cuajimalpa, Avenida Pedro Antonio de los Santos 84, 11850 México D. F., México

Received: May 21, 2009; Revised Manuscript Received: November 22, 2009

Schiff bases bearing an intramolecular hydrogen bond are known to undergo excited-state intramolecular proton transfer and $E-Z$ isomerization, which are related to their thermochromism and solvatochromism properties. In this study, we explored these ultrafast photoinduced processes for two doubly hydroxylated Schiff bases, salicylidene-2-aminophenol and 2-hydroxynaphthylmethylidene-2-aminophenol. From comparisons with our previously reported results for the parent monohidroxylated Schiff base salicylideneaniline, we were able to establish the lack of an effect of a second intramolecular hydrogen bond in the excited-state intramolecular proton-transfer process. Moreover, we synthesized and studied the photophysics of 14 diphenyl-tin^{IV} derivatives with Schiff bases with the same framework as the former two. In these organometallic compounds, we observed an increase of more than 50 times in the excited-state decay times in comparison with those of the free ligands. This finding is attributed to the coordination with the metallic center, which restricts the fluctuations of the geometry of the organic Schiff base skeleton. The emission bands of these complexes can be easily tuned through substitutions at the Schiff base ligand and can be made to be centered well above 600 nm. The much enhanced emissive behavior of all diphenyl-tin^{IV} derivatives allowed the study of several properties of their electronically excited states, including the effects of different substituents on their femtosecond and picosecond dynamics. Considering potential applications, we also performed transient absorption experiments to assess the wavelength interval for stimulated emission of this type of compound. Finally, we determined their two-photon absorption cross sections in the 760−820-nm range by measuring their two-photon induced fluorescence excitation spectra. Mainly, our results illustrate that the diphenyl-tin^{IV} moiety, thanks to its size and its coordination mode with a single Schiff base, can be coordinated to this versatile framework to obtain tunable optical properties wherein the emissive states can have lifetimes on the nanosecond time scale.

Introduction

Schiff bases bearing an intramolecular hydrogen bond have been extensively used as model systems to study fundamental photophysical processes such as excited-state intramolecular proton transfer (ESIPT), photochromism, solvatochromism, and thermochromism.[1–13] Among these compounds, salicylidene-*ortho*-aminophenols and related Schiff bases have been further targeted and studied because, in addition to the above-mentioned characteristics, they also have the ability to act as versatile chelating ligands.[14] Some derivatives with this type of Schiff base have found important applications, as they have been considered as molecular switches,[15] as materials with nonlinear optical properties,[16–19] and as components in the construction of organic light-emitting devices (OLEDs).[20–24]

Upon chelation, the photophysical features of the metallic derivatives are vastly different from those of the free ligands, where the most notorious, in some cases, is an improvement of their fluorescent character.[14,25–30] Here, it is worth emphasizing that, although the fluorescence from Schiff bases is extremely weak because of their fast excited-state decay processes,[1–8] the inclusion of a metallic center can dramatically enhance their fluorescence (with the exception of some compounds bearing heavy metals, because they can, in principle, promote singlet−triplet mixing, also known as the "heavy-atom effect").[20,31]

There are several examples of fluorescent derivatives of similar systems (where two aromatic groups in the ligand are joined through a section that includes a double bond[14,20–30,32,33]). However, more studies are needed to determine the specific effects of different and more versatile metallic centers in the luminescent properties. This is important because the chelating center will determine the degree of charge-transfer character of the electronic excitation, as well as the extent of the electronic delocalization in the molecule. In this context, we have carried out a systematic study aimed to determine how the bonding to a tin metal center changes the photophysical properties of the basic salicylidene-*ortho*-aminophenol organic framework. The present analysis also describes the contrast between the photophysics of the two doubly hydroxylated Schiff bases ("free ligands") salicylidene-2-aminophenol (**1**) and 2-hydroxynaphthylmethylidene-2-aminophenol (**2**), and the derivatives they form when bis-chelating a diphenyl-tin^{IV} unit (**3** and **4** series, respectively; see Scheme 1). As will be shown, the diphenyl-

* To whom correspondence should be addressed. E-mail: jpeon@servidor.unam.mx.
[†] Universidad Nacional Autónoma de México.
[‡] UAM-Cuajimalpa.

10.1021/jp904784b
Published on Web 12/28/2009

SCHEME 1: (a) Structures and Atom Numbering of the Free Schiff Bases (1 and 2) and Corresponding Diphenyl-Tin^{IV} Derivatives (3a−g and 4a−g) of This Study and (b) Plane Angle Measurement of Structurally Available Schiff Bases

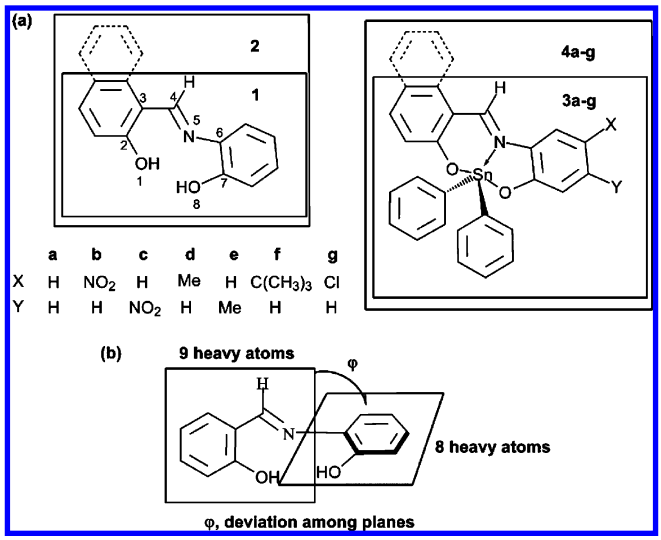

tin^{IV} moiety is a chelation center with a very appropriate size for a three-center interaction with a single Schiff base, making it an adaptable system for designing multichromophoric systems. In particular, diphenyl-tin^{IV} chelation allows the tuning of the position of the emission band in an easy-to-synthesize system through changes in the substitutions at the Schiff base skeleton. We also show that, although the large nuclear charge of the tin atom could, in principle, accelerate the complexes' S_1 decay due to intersystem crossing,[20,31] these molecules have dramatically increased fluorescence lifetimes in comparison with those of the free bases because of the restrictions of their structural fluctuations.

We chose a diphenyl-tin^{IV} moiety based on the fact that, in contrast to what happens with dimethyl-tin^{IV}, di-*n*-butyl-tin^{IV}, and other nonaromatic diorganil-tin^{IV} groups that usually lead to the formation of dimeric and other supramolecular coordination species, the compounds resulting from chelation of a diphenyl-tin^{IV} fragment by Schiff bases have the desirable feature that they remain as monomers, thus facilitating their spectroscopic and physicochemical analysis.[16,34–41] The consideration of a chelation center with two extra organometallic bonds (to phenyl groups in this case) also indicates the possibility of using these extra positions for combined effects in future multichromophoric systems (synthetically, the tin^{IV} center is ideal for this purpose).

To fully compare the photophysics of the ligands with those of the derivatives, we performed both steady-state and time-resolved experiments. With the steady-state measurements, we analyzed the influence that different substituents placed at the aminophenol (aniline) ring have on the electronic transitions of the derivatives (**3** and **4** series). With time-resolved fluorescence up-conversion experiments, we were able to determine that the improved rigidity of the Schiff base framework in the **3**- and **4**-series diphenyl-tin^{IV} compounds produces a remarkable increase (of more than 50 times) in the fluorescence lifetimes with respect to the analogous free Schiff bases. Thinking about future possible applications such as the construction of organic light-emitting devices (OLEDs), we also examined the excited-state dynamics through femtosecond transient absorption for one representative tin^{IV} derivative (**4d**). Such measurements allowed us to distinguish the spectral region where the $S_1 \rightarrow S_0$ stimulated emission can be observed, in contrast to excited singlet-to-singlet state absorption ($S_n \leftarrow S_1$). Finally, taking advantage of their highly emissive character, we measured the two-photon absorption cross sections (TPACSs) of the **3**- and **4**-series compounds, by monitoring their two-photon excitation fluorescence (TPEF).

Experimental Methods

2-Hydroxy-1-naphthaldehyde was supplied from Aldrich and recrystallized from ethanol. All other reactants were purchased from Aldrich and used without further purification. The solution NMR characterization experiments were performed on a Bruker 300 spectrometer at room temperature. The ^{1}H NMR spectra were recorded at 300.13 MHz using a spectral width of 6200 Hz and an acquisition time of 2.64 s. In all cases, the spectra were obtained using 16384 data points, a 45° pulse width, and 16 scans. The ^{13}C NMR spectra were recorded at 75.468 MHz using a spectral width of 17360 Hz and an acquisition time of 2.50 s, with 16384 data points and at least 1024 scans. The ^{119}Sn spectra were recorded at 100.726 MHz using a spectral width of 10080 Hz, an acquisition time of 0.4 s, 16384 data points, and at least 1024 scans. The direct observation of 2D NMR spectra was performed through (^{13}C−^{1}H) heteronuclear correlation (HETCOR), (^{1}H−^{1}H) correlation spectroscopy (COSY) experiments using standard Bruker pulse sequences. The chemical shifts (ppm) are relative to TMS [$\delta(^1\text{H}) = 0.00$ and $\delta(^{13}\text{C}) = 0.0$ ppm] and $SnMe_4$ [$\delta(^{119}\text{Sn}) = 0.0$ ppm], and coupling constants are quoted in hertz. Infrared spectra were recorded as KBr pellets on a Bruker Tensor 27 FT-IR spectrophotometer. Melting points were measured on a Fisher-Johns apparatus and were not corrected. Mass spectrometry determinations through the fast atom bombardment (FAB^+) technique were made on a JEOL SX-102A spectrometer using a *meta*-nitrobenzylic alcohol matrix.

Synthesis of 1 and 2: General Procedure. Equimolar amounts of salicylaldehyde (for **1**) or 2-hydroxy-1-naphthaldehyde (for **2**) and 2-aminophenol were refluxed in methanol for 1.5 h with azeotropic removal of water. Compounds **1** and **2** were obtained as solid precipitates and recrystallized twice from a methylene chloride−methanol solution; their purities were verified by thin-layer chromatography on Silufol UV sheets using ethyl acetate, methylene chloride, and methanol as mobile phases. ^{1}H NMR structural characterization and physical properties were compared with those reported elsewhere.[23,42]

Synthesis of 3a−g and 4a−g: General Procedure. Equimolar amounts of diphenyl-tin^{IV} oxide, salicylaldehyde (for **3a−g**) or 2-hydroxy-1-naphthaldehyde (for **4a−g**), and the corresponding *ortho*-aminophenol (**a**, 2-aminophenol; **b**, 2-amino-4-nitrophenol; **c**, 2-amino-5-nitrophenol; **d**, 2-amino-*para*-cresol; **e**, 6-amino-*meta*-cresol; **f**, 2-amino-4-*tert*-butylphenol; **g**, 2-amino-4-chlorophenol) were maintained in ethanol reflux for 12 h under azeotropic removal of water. All compounds were isolated as solids after reduced-pressure distillation of the ethanol; recrystallized from a 1:5 mixture of dichloromethane and ethanol; and then characterized by ^{1}H, ^{13}C, 2D (HETCOR and COSY), and ^{119}Sn NMR spectroscopies. For **3a−g**, all data resemble those reported previously.[35,43] The yields, melting points, IR, NMR, mass spectrometry (FAB^+), and elemental analysis data for **4a−g** are reported in the following paragraphs. Purities were verified by thin-layer chromatography on Silufol UV254 sheets using ethanol as the mobile phase, as well as by comparison between steady-state fluorescence excitation and absorption spectra.

2,2-Diphenyl-6-aza-1,3-dioxa-2-stanna[*d*]benzo[1,2-*h*]naphthocyclononene (4a). Red crystals, yield 88%, mp 208−210 °C. IR (*ν*) (KBr): 3051, 1593 (C═N), 1538, 1471, 1396, 1306, 1175, 1073, 982, 830, 739, 699, 613 (Sn−C), 558 (Sn−O), 449 (Sn−N) cm^{-1}. ^1H NMR (*δ*, ppm, $CDCl_3$): 9.39 (1H, H7), 7.94 (4H, H_{ortho}), 7.42 (1H, H16), 7.78 (1H, H11), 7.58 (1H, H13), 7.38 (4H, H_{meta}), 7.37 (1H, H15), 7.36 (2H, H_{para}), 7.31 (1H, H20), 7.22 (1H, H18), 7.18 (1H, H10), 7.17 (1H, H14), 7.12 (1H, H21), 6.71 (1H, H19). ^{13}C NMR (*δ*, ppm, $CDCl_3$): 172.6 (C9), 158.6 (C7), 156.0 (C4), 139.5 (C_{ipso}), 138.9 (C11), 136.4 (C_{ortho}), 134.1 (C17), 132.6 (C5), 130.6 (C_{para}), 129.5 (C13), 129.4 (C20), 128.7 (C_{meta}), 128.5 (C15), 127.3 (C12), 124.8 (C14), 123.6 (C10), 118.7 (C21), 118.6 (C16), 117.0 (C19), 114.7 (C18), 109.1 (C8). ^{119}Sn NMR (*δ*, ppm): −325.7 ($CDCl_3$), −420.2 (DMSO-d_6). MS-FAB *m*/*z* (%): 535 $M^+[^{120}Sn]$ (20), 533 $M^+[^{118}Sn]$ (15), 531 $M^+[^{116}Sn]$ (7), 458 $M^+[^{120}Sn]$ − Ph (5), 456 $M^+[^{118}Sn]$ − Ph (4), 454 $M^+[^{116}Sn]$ − Ph (3), 391 (10), 380 $M^+[^{120}Sn]$ − $C_{12}H_{11}$ (5), 378 $M^+[^{118}Sn]$ − $C_{12}H_{11}$ (3), 376 $M^+[^{116}Sn]$ − $C_{12}H_{11}$ (1), 307 (35), 289 (17), 154 (100), 136 (61), 107 ($[C_7H_7O^+]$) (17), 89 ($[C_4H_9O_2^+]$) (15), 77 ($[C_6H_5^+]$) (13). Elemental analysis. Found (%): C, 65.15; H, 3.88; N, 2.66. Calculated for $C_{29}H_{21}NO_2Sn$ (%): C, 65.20; H, 3.96; N, 2.62.

2,2-Diphenyl-6-aza-1,3-dioxa-15-nitro-2-stanna[*d*]benzo[1,2-*h*]naphthocyclononene (4b). Red powder, yield 93%, mp 234−236 °C. IR (*ν*) (KBr): 3070, 1597 (C═N), 1536, 1501, 1430, 1386, 1304, 1164, 1080, 991, 834, 746, 698 (Sn−C), 594 (Sn−O), 488, 450 (Sn−N) cm^{-1}. ^1H NMR (*δ*, ppm, $CDCl_3$): 9.57 (1H, H7), 8.36 (1H, H18), 8.19 (1H, H16), 8.07 (1H, H20), 7.97 (1H, H11), 7.89 (4H, H_{ortho}), 7.74 (1H, H13), 7.61 (1H, H15), 7.45−7.40 (6H, H_{meta}, H_{para}), 7.39 (1H, H14), 7.25 (1H, H10), 7.12 (1H, H21). ^{13}C NMR (*δ*, ppm, $CDCl_3$): 174.1 (C9), 164.8 (C4), 157.8 (C7), 140.9 (C11), 138.1 (C_{ipso}), 137.9 (C19), 136.2 (C_{ortho}), 133.9 (C17), 132.5 (C5), 130.8 (C_{para}), 129.7 (C13), 129.3 (C15), 129.0 (C_{meta}), 127.4 (C12), 125.3 (C20), 124.6 (C10), 124.4 (C14), 119.0 (C16), 118.1 (C21), 111.5 (C18), 109.4 (C8). ^{119}Sn NMR (*δ*, ppm): −316.9 ($CDCl_3$), −417.1 (DMSO-d_6). MS-FAB *m*/*z* (%): 580 $M^+[^{120}Sn]$ (9), 578 $M^+[^{118}Sn]$ (7), 576 $M^+[^{116}Sn]$ (3), 503 $M^+[^{120}Sn]$ − Ph (3), 501 $M^+[^{118}Sn]$ − Ph (2), 499 $M^+[^{116}Sn]$ − Ph (1), 391 (6), 307 (27), 289 (14), 154 (100), 136 (67), 107 ($[C_7H_7O^+]$) (21), 89 ($[C_4H_9O_2^+]$) (21), 77 ($[C_6H_5^+]$) (19). Elemental analysis. Found (%): C, 59.99; H, 3.49; N, 4.81. Calculated for $C_{29}H_{20}N_2O_4Sn$ (%): C, 60.14; H, 3.48; N, 4.84.

2,2-Diphenyl-6-aza-1,3-dioxa-16-nitro-2-stanna[*d*]benzo[1,2-*h*]naphthocyclononene (4c). Red powder, yield 90%, mp > 290 °C. IR (*ν*) (KBr): 3048, 1602 (C═N), 1568, 1539, 1515, 1475, 1432, 1384, 1336, 1315, 1278, 1145, 1073, 873, 835, 816, 741, 699 (Sn−C), 578 (Sn−O), 452 (Sn−N) cm^{-1}. ^1H NMR (*δ*, ppm, $CDCl_3$): 9.60 (1H, H7), 8.08 (1H, H16), 8.00 (1H, H11), 7.89 (4H, H_{ortho}), 7.87 (1H, H18), 7.76 (1H, H13), 7.65 (1H, H19), 7.58 (1H, H15), 7.57 (1H, H20), 7.56 (1H, H21), 7.42−7.40 (6H, H_{meta}, H_{para}), 7.39 (1H, H14), 7.24 (1H, H10). ^{13}C NMR (*δ*, ppm, $CDCl_3$): 174.0 (C9), 157.8 (C7), 155.1 (C4), 147.1 (C20), 140.4 (C11), 138.1 (C_{ipso}), 135.6 (C_{ortho}), 134.2 (C17), 133.8 (C5), 130.0 (C_{para}), 129.1 (C13), 128.6 (C15), 128.3 (C_{meta}), 127.1 (C12), 124.1 (C10), 123.8 (C14), 118.4 (C16), 114.5 (C21), 112.4 (C18), 111.6 (C19), 109.1 (C8). ^{119}Sn NMR (*δ*, ppm): −322.5 ($CDCl_3$), −414.6 (DMSO-d_6). MS-FAB *m*/*z* (%): 580 $M^+[^{120}Sn]$ (11), 578 $M^+[^{118}Sn]$ (8), 576 $M^+[^{116}Sn]$ (4), 503 $M^+[^{120}Sn]$ − Ph (4), 501 $M^+[^{118}Sn]$ − Ph (2), 499 $M^+[^{116}Sn]$ − Ph (1), 391 (21), 307 (24), 289 (14), 154 (100), 136 (73), 107 ($[C_7H_7O^+]$) (23), 89 ($[C_4H_9O_2^+]$) (24), 77 ($[C_6H_5^+]$) (24). Elemental analysis. Found (%): C, 60.34; H, 3.51; N, 4.92. Calculated for $C_{29}H_{20}N_2O_4Sn$ (%): C, 60.14; H, 3.48; N, 4.84.

2,2-Diphenyl-6-aza-1,3-dioxa-15-methyl-2-stanna[*d*]benzo[1,2-*h*]naphthocyclononene (4d). Red powder, yield 94%, mp 205−208 °C. IR (*ν*) (KBr): 3052, 3028, 1602 (C═N), 1534, 1493, 1471, 1291, 1193, 1150, 840, 813, 757, 735, 701 (Sn−C), 536 (Sn−O), 443 (Sn−N) cm^{-1}. ^1H NMR (*δ*, ppm, $CDCl_3$): 9.47 (1H, H7), 7.98 (1H, H16), 7.93 (4H, H_{ortho}), 7.84 (1H, H11), 7.66 (1H, H13), 7.48 (1H, H15), 7.38−7.37 (6H, H_{meta}, H_{para}), 7.28 (1H, H10), 7.22 (1H, H14), 7.19 (1H, H21), 7.04 (2H, H18, H20), 2.32 (3H, H34). ^{13}C NMR (*δ*, ppm, $CDCl_3$): 172.5 (C9), 156.4 (C4), 155.7 (C7), 139.5 (C_{ipso}), 138.7 (C11), 136.5 (C_{ortho}), 134.1 (C17), 132.1 (C5), 130.6 (C20), 130.3 (C_{para}), 129.5 (C13), 128.7 (C_{meta}), 128.5 (C15), 127.4 (C12), 126.4 (C19), 124.9 (C14), 123.6 (C10), 118.8 (C16), 118.4 (C21), 115.0 (C18), 109.2 (C8), 20.9 (C34). ^{119}Sn NMR (*δ*, ppm): −324.4 ($CDCl_3$), −399.0 (DMSO-d_6). MS-FAB *m*/*z* (%): 549 $M^+[^{120}Sn]$ (21), 547 $M^+[^{118}Sn]$ (16), 545 $M^+[^{116}Sn]$ (7), 472 $M^+[^{120}Sn]$ − Ph (5), 470 $M^+[^{118}Sn]$ − Ph (3), 468 $M^+[^{116}Sn]$ − Ph (2), 394 $M^+[^{120}Sn]$ − $C_{12}H_{11}$ (5), 392 $M^+[^{118}Sn]$ − $C_{12}H_{11}$ (4), 390 $M^+[^{116}Sn]$ − $C_{12}H_{11}$ (1), 391 (8), 307 (26), 289 (13), 154 (100), 136 (61), 107 ($[C_7H_7O^+]$) (18), 89 ($[C_4H_9O_2^+]$) (17), 77 ($[C_6H_5^+]$) (15). Elemental analysis. Found (%): C, 64.89; H, 4.81; N, 2.46. Calculated for $C_{30}H_{23}NO_2Sn\cdots C_2H_5OH$ (%): C, 64.67; H, 4.92; N, 2.36.

2,2-Diphenyl-6-aza-1,3-dioxa-16-methyl-2-stanna[*d*]benzo[1,2-*h*]naphthocyclononene (4e). Red powder, yield 80%, mp 177−179 °C. IR (*ν*) (KBr): 3064, 2917, 1606 (C═N), 1539, 1491, 1454, 1432, 1397, 1366, 1307, 1183, 1073, 979, 862, 828, 735, 698 (Sn−C), 574 (Sn−O), 482, 448 (Sn−N) cm^{-1}. ^1H NMR (*δ*, ppm, $CDCl_3$): 9.29 (1H, H7), 7.95 (4H, H_{ortho}), 7.81 (1H, H16), 7.73 (1H, H11), 7.53 (1H, H13), 7.39 (1H, H15), 7.42−7.38 (6H, H_{meta}, H_{para}), 7.16 (1H, H10), 7.15 (H18), 7.14 (1H, H14), 6.94 (1H, H21), 6.49 (1H, H19). ^{13}C NMR (*δ*, ppm, $CDCl_3$): 172.0 (C9), 158.3 (C4), 154.9 (C7), 139.8 (C20), 139.6 (C_{ipso}), 138.4 (C11), 136.5 (C5), 136.4 (C_{ortho}), 134.0 (C17), 130.2 (C_{para}), 129.3 (C13), 128.6 (C_{meta}), 128.3 (C15), 127.5 (C12), 124.7 (C10), 123.4 (C14), 119.0 (C21), 118.7 (C16), 118.0 (C19), 114.2 (C18), 109.0 (C8), 21.4 (C34). ^{119}Sn NMR (*δ*, ppm): −325.9 ($CDCl_3$), −421.1 (DMSO-d_6). MS-FAB *m*/*z* (%): 549 $M^+[^{120}Sn]$ (23), 547 $M^+[^{118}Sn]$ (17), 545 $M^+[^{116}Sn]$ (9), 472 $M^+[^{120}Sn]$ − Ph (5), 470 $M^+[^{118}Sn]$ − Ph (3), 468 $M^+[^{116}Sn]$ − Ph (2), 394 $M^+[^{120}Sn]$ − $C_{12}H_{11}$ (5), 392 $M^+[^{118}Sn]$ − $C_{12}H_{11}$ (5), 390 $M^+[^{116}Sn]$ − $C_{12}H_{11}$ (1), 391 (20), 307 (32), 289 (18), 154 (100), 136 (66), 107 ($[C_7H_7O^+]$) (23), 89 ($[C_4H_9O_2^+]$) (23), 77 ($[C_6H_5^+]$) (23). Elemental analysis. Found (%): C, 64.75; H, 4.87; N, 2.48. Calculated for $C_{30}H_{23}NO_2Sn\cdots C_2H_5OH$ (%): C, 64.67; H, 4.92; N, 2.36.

2,2-Diphenyl-6-aza-1,3-dioxa-15-*tert*-butyl-2-stanna[*d*]benzo[1,2-*h*]naphthocyclononene (4f). Red powder, yield 86%, mp 236−240 °C. IR (*ν*) (KBr): 3049, 2954, 1600 (C═N), 1538, 1491, 1458, 1427, 1396, 1362, 1303, 1279, 1192, 1098, 1072, 830, 739, 699 (Sn−C), 557 (Sn−O), 496, 446 (Sn−N) cm^{-1}. ^1H NMR (*δ*, ppm, $CDCl_3$): 9.49 (1H, H7), 7.95 (4H, H_{ortho}), 7.94 (1H, H16), 7.82 (1H, H11), 7.65 (1H, H13), 7.48 (1H, H15), 7.38 (1H, H18), 7.37−7.34 (6H, H_{meta}, H_{para}), 7.29 (1H, H20), 7.27 (1H, H14), 7.21 (1H, H10), 7.10 (1H, H21), 1.36 (9H, H35, H36, H37). ^{13}C NMR (*δ*, ppm, $CDCl_3$): 172.4 (C9), 156.3 (C4), 155.6 (C7), 140.0 (C19), 139.4 (C_{ipso}), 138.7 (C11), 136.5 (C_{ortho}), 134.1 (C17), 131.3 (C5), 130.2 (C_{para}), 129.5 (C13), 128.7 (C_{meta}), 128.5 (C15), 127.4 (C12), 126.8 (C20), 124.9 (C10), 123.6 (C14), 118.6 (C16), 118.1 (C21), 111.2 (C18), 109.2 (C8), 34.3 (C34), 31.6 (C35, C36, C37). ^{119}Sn NMR (*δ*, ppm): −321.9 ($CDCl_3$), −391.8 (DMSO-d_6). MS-FAB *m*/*z* (%): 591 $M^+[^{120}Sn]$ (21), 589 $M^+[^{118}Sn]$ (15), 587 $M^+[^{116}Sn]$ (7), 514 $M^+[^{120}Sn]$ − Ph (4), 512 $M^+[^{118}Sn]$ − Ph (3), 510

$M^+[^{116}Sn] - Ph$ (1), 422 $M^+[^{120}Sn] - C_{13}H_{13}$ (4), 420 $M^+[^{118}Sn] - C_{13}H_{13}$ (3), 418 $M^+[^{116}Sn] - C_{13}H_{13}$ (2), 391 (6), 307 (29), 289 (13), 154 (100), 136 (62), 107 [$C_7H_7O^+$] (17), 89 [$C_4H_9O_2^+$] (16), 77 [$C_6H_5^+$] (13). Elemental analysis. Found (%): C, 67.22; H, 4.86; N, 2.43. Calculated for $C_{33}H_{29}NO_2Sn$ (%): C, 67.14; H, 4.95; N, 2.37.

2,2-Diphenyl-6-aza-1,3-dioxa-15-chloro-2-stanna[*d*]benzo[1,2-*h*]naphthocyclononene (4g). Brown powder, yield 82%, mp > 290 °C. IR (ν) (KBr): 3054, 3032, 1596 (C═N), 1535, 1471, 1427, 1393, 1363, 1295, 1197, 1074, 914, 832, 794, 739, 699 (Sn—C), 555 (Sn—O), 523, 493, 454 (Sn—N) cm^{-1}. ^1H NMR (δ, ppm, $CDCl_3$): 9.28 (1H, H7), 7.90 (4H, H_{ortho}), 7.87 (1H, H16), 7.81 (1H, H11), 7.59 (1H, H13), 7.43 (1H, H15), 7.39−7.35 (4H, H_{meta}, H_{para}), 7.26 (1H, H18), 7.21 (1H, H14), 7.17 (1H, H10), 7.13 (1H, H20), 7.03 (1H, H21). ^{13}C NMR (δ, ppm, $CDCl_3$): 173.2 (C9), 157.1 (C4), 156.4 (C7), 139.6 (C11), 139.1 (C_{ipso}), 136.4 (C_{ortho}), 134.0 (C17), 133.3 (C5), 130.4 (C_{para}), 129.5 (C13), 129.0 (C20), 128.8 (C_{meta}), 128.7 (C15), 127.4 (C12), 124.8 (C10), 123.9 (C14), 121.6 (C19), 119.5 (C21), 118.8 (C16), 114.9 (C18), 109.2 (C8). ^{119}Sn NMR (δ, ppm): −321.5 ($CDCl_3$), −406.3 (DMSO-d_6). MS-FAB *m*/*z* (%): 569 $M^+[^{120}Sn]$ (40), 567 $M^+[^{118}Sn]$ (30), 565 $M^+[^{116}Sn]$ (14), 492 $M^+[^{120}Sn] - Ph$ (10), 490 $M^+[^{118}Sn] - Ph$ (8), 488 $M^+[^{116}Sn] - Ph$ (4), 415 $M^+[^{120}Sn] - Ph_2$ (9), 413 $M^+[^{120}Sn] - Ph_2$ (8), 411 $M^+[^{118}Sn] - Ph_2$ (4), 391 (12), 307 (25), 289 (14), 154 (100), 136 (68), 107 [$C_7H_7O^+$] (22), 89 [$C_4H_9O_2^+$] (23), 77 [$C_6H_5^+$] (20). Elemental analysis. Found (%): C, 61.20; H, 3.65; N, 2.52. Calculated for $C_{29}H_{20}ClNO_2Sn$ (%): C, 61.25; H, 3.55; N, 2.46.

Steady-State Spectroscopy. Stationary absorption spectra were recorded with a Cary-50 spectrophotometer (Varian). Steady-state fluorescence emission and excitation spectra were measured on a Cary Eclipse spectrophotometer (Varian) and were always performed on solutions with optical densities less than or equal to 0.05. All measurements were performed at room temperature (20 ± 1 °C) in HPLC- (high-performance-liquid-chromatography-) quality solvents.

Fluorescence Quantum Yields. To avoid self-absorption of emitted fluorescence and ensure linear behavior, diluted solutions (about 4 μM) of diphenyl-tin^{IV} derivatives with Schiff bases in HPLC-grade ethanol were used to record steady-state fluorescence emission spectra at two different excitation wavelengths (355 and 490 nm). Fluorescence quantum yields (ϕ) were estimated with reference to rhodamine B (RhB) in methanol.[44] The RhB standard was purchased from Aldrich and recrystallized from methylene chloride. Steady-state fluorescence emission spectra of 0.44 μM solutions of RhB in methanol were acquired at the same two excitation wavelengths as the **3** and **4** series. The fluorescence quantum yield of RhB in methanol (ϕ_R) was taken as 0.70.[44] Measurements of fluorescence at each excitation wavelength and optical densities of all compounds were recorded in triplicate using a 1-cm quartz cell. We found typical percentage errors in ϕ of 10%. Fluorescence quantum yields of compounds **1** and **2** were measured in a similar way, by direct excitation of the *E*-OH form (355 nm).

Time-Resolved Spectroscopy. Our experimental up-conversion technique has been previously reported.[7] Briefly, a pulsed beam with a repetition rate of 100 MHz, generated in a Ti:sapphire oscillator pumped by a 5-W Verdi V5 laser (Coherent Inc.), was passed through a fused-silica prism compressor before it was frequency-doubled in a 0.5-mm BBO (BaB_2O_4) crystal. The second harmonic was passed through a half-wave plate to control its polarization to magic-angle conditions and then focused into a 1-mm-path-length flow quartz cell containing the sample solution. Fluorescence was collected with a pair of parabolic mirrors and refocused to another 0.5-mm BBO crystal, where it was crossed at its focal point with the remaining and temporally delayed fundamental gate beam. The resultant frequency-mixing signal was finally focused into a double monochromator (Oriel) and detected with a photomultiplier tube. The instrument response function was determined by time-resolving the Raman scattering of the solvent and was found to be Gaussian with full widths at half maxima of 190 ± 5, 210 ± 5, and 220 ± 5 fs for setups resolving fluorescence at 422, 390, and 385 nm, respectively.

For transient absorption experiments, the pulsed beam at the output of the Ti:sapphire oscillator was passed through a regenerative amplification system to yield 0.3 mJ pulses at a repetition rate of 1 kHz. Following a previously reported procedure,[45] the pump at 400 nm was generated in a 0.5-mm β-BBO crystal and separated from the remaining fundamental with a dichroic mirror (CVI), after which it was passed through a half-wave plate to adjust to magic angle conditions, and finally focused at the sample with a 15-cm fused-silica lens. A portion of the remaining fundamental was passed through a 1-mm Z-cut sapphire plate to generate a white light continuum probe beam that was sent to a delay stage before it was focused in the sample. The relative spot sizes of the probe and pump beams (200 and 20 μm, correspondingly) ensured that the focused probe light was homogeneously overlapped with the excitation pulses for the full spectral range of our experiments. Our setup used single-channel detection where a double 10-cm monochromator was set to a particular wavelength to acquire the transient transmittance change through the use of a diode, an optical chopper in the path of the pump beam, and a lock-in amplifier. The probe light intensity (I_0) was determined in a separate measurement with the pump beam blocked and with the chopper directly modulating the intensity of the probe beam. The instrument response function for transient absorption measurements was found to be Gaussian with a 400-fs full width at half-maximum.[45]

Two-Photon Absorption Cross Sections (TPACSs). To determine TPACSs, we followed the two-photon-induced fluorescence measurement technique,[46–48] using a constantly refreshed 10 μM solution of recrystallized RhB in HPLC-grade methanol solution as the reference. To produce TPEF, we used a Ti:sapphire oscillator pumped by a 5-W Verdi V5 continuous laser (Coherent Inc.) to generate a 83 MHz, femtosecond pulsed train. The obtained 750−890-nm tunable pulsed beam was passed through a fused-silica compressor and a half-wave plate, followed by a calcite Glan−Taylor polarizer before it was split by a neutral-density filter. The less intense branch was passed through a chopper and then focused into a silicon diode connected to an oscilloscope (Agilent) to continuously check the intensity of the beam. To determine the correspondence between the voltage and the power of the beam, we made a linear regression study at every excitation wavelength used. Power values were taken for intensities at which the power-meter resolution was accurate, and then its linear behavior with respect to voltage was verified.

The remaining beam branch was focused into the center of a stoppered 1-cm-path-length quartz cell containing the sample. To ensure homogeneity of the solutions and avoid erroneous measurements due to photobleaching, a small magnetic stirrer was introduced into the cell so the samples were constantly stirred. Because of this, small amounts of dust had to be avoided because they could cause an abnormally high value of the detected TPEF. To achieve this goal, we filtered every solution

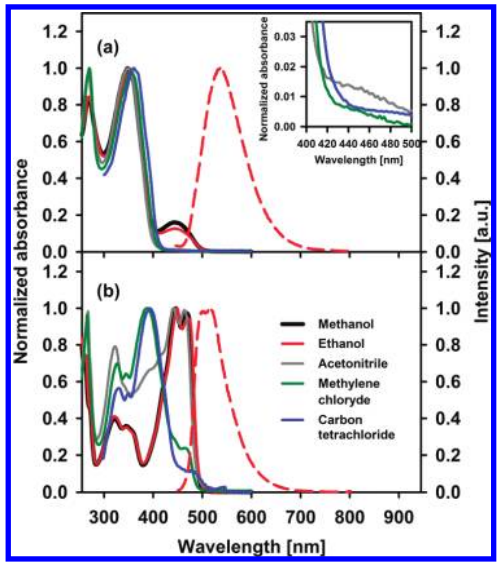

Figure 1. Stationary absorption (solid lines) and fluorescence spectra (dashed line) of (a) **1** and (b) **2** in different solvents. Fluorescence spectra were recorded upon excitation at 355 nm.

through 0.45-μm nylon filters (Millipore) supported in 2.5-cm-diameter swinnex filter holders (Millipore). The resulting TPEF was collimated and continuously collected by a UV−vis portable spectrophotometer (Ocean Optics) with variable integration time, situated perpendicular to the incident beam. Because TPACSs were measured relative to a standard, every sample measurement was taken between two measurements of RhB reference solution; each time, five values were recorded, and they were all measured by recording the intensity of the TPEF spectra at the fluorescence maximum. To estimate typical percentage error, four randomly chosen diphenyl-tin^{IV} derivatives were measured in duplicate. We found typical percentage errors in TPACSs of 15%. To ensure a biphotonic excitation process, we verified the TPEF squared dependence on beam intensity for four randomly chosen derivatives.

Photodegradation of the samples was monitored by stationary absorption spectra taken both before and after TPEF was induced. Compounds **3a**−**g** and **4a**−**g** were dissolved in HPLC-grade ethanol, and the resulting solutions had concentrations of around 0.1 mM. Exact molarities were calculated with the stationary absorption spectra.

Results and Discussion

Steady-State Spectroscopy. The stationary absorption spectra of the dihydroxylated free Schiff bases **1** and **2** in different solvents are shown in Figure 1, where we also include their steady-state emission spectra in ethanol. From comparison with similar systems,[1–9,11–13] for both Schiff bases, the absorption band at shorter wavelengths can be assigned to the $S_1 \leftarrow S_0$ transition of the *E*-enolimine isomer (*E*-OH; see Scheme 2 for isomer visualizations). In **1**, solvatochromism is noticeable only in protic solvents such as methanol and ethanol, where the shoulder centered at 450 nm indicates the $S_1 \leftarrow S_0$ absorption of the *Z*-ketoenamine form (*Z*-NH).[1–9,11–13] In contrast, **2** exhibits a more marked solvatochromic effect. Here, the band at 380 nm corresponding to the *E*-OH form is prominent only in carbon tetrachloride and methylene chloride, and it decreases in more polar solvents with the simultaneous increase of absorption at wavelengths above 400 nm, indicating the shift of the tautomeric equilibrium toward the *Z*-NH isomer.

As has been discussed elsewhere,[9,12] solvent polarity is not a unique parameter to explain these solvatochromic effects,

SCHEME 2: Energy Diagram and Electronic Transitions Involved in the Photoinduced Cycle of the Free Schiff Bases under Study[a,b]

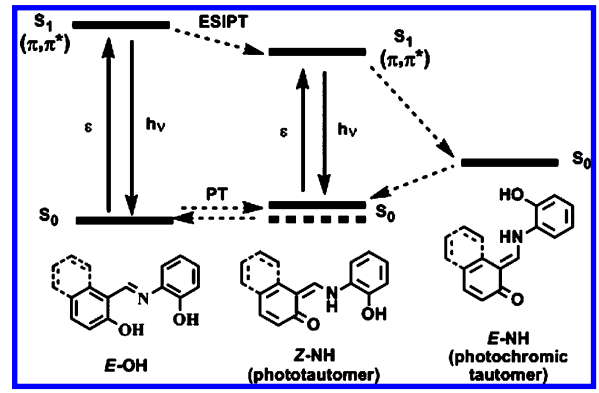

[a] The ε and $h\nu$ labels indicate absorption and fluorescence emission, respectively. [b] The S_0 state of the *Z*-NH (*Z*-ketoenamine) tautomer is represented by two different lines: The upper solid line indicates solvent−solute combinations in which the *Z*-NH isomer is less stable at room temperature and its steady-state absorption band at ~450 nm is rather small (e.g., **1** in methylene chloride), whereas the lower dashed line refers to the cases in which a ground-state equilibrium between the *E*-OH (*E*-enolimine) and *Z*-NH forms can be reached at room temperature (e.g., **1** in methanol).

because the tautomeric shift toward the *Z*-NH form is not necessarily determined by a high dielectric constant of the solvent. Instead, the solvatochromic effect on Schiff bases must be explained by means of both intramolecular and specific solvent−solute interactions. Hence, in **1**, the intramolecular hydrogen bond in the *E*-OH tautomer is sufficiently stable to predominate in all solvents. Only the alcohol solvents allow, to a small extent, the formation of the *Z*-NH isomer by stabilizing it with a particular hydrogen-bond network. In contrast, the *Z*-NH form of **2** is more easily formed. The overall preference for the *E*-OH form of **1** versus the preference for the *Z*-NH isomer of **2** presumably lies in the fact that the loss of aromaticity when going from the *E*-OH to the *Z*-NH form in **2** is compensated by the other aromatic ring of the naphthalene system.[10,13]

The steady-state emissions of **1** and **2** are largely Stokes-shifted with respect to the *E*-OH absorption bands (Figure 1), even upon direct excitation of this last isomer. In agreement with other Schiff bases, this supports the fact that the dominant fluorescence signal comes from the *Z*-NH isomer that is formed after an ESIPT from the *E*-OH local excited state.[1–9,11–13] We estimated the fluorescence quantum yields of **1** and **2** in ethanol as 0.003 ± 0.001 and 0.005 ± 0.001, respectively, under direct excitation of the *E*-OH form. These values are consistent with the typical low yields of Schiff bases with intramolecular hydrogen bonds,[6,8,13] accounting for fast depletion channels occurring in the excited state.

In contrast with the free Schiff bases, the diphenyl-tin^{IV} derivatives (series **3** and **4**) have significantly higher fluorescence quantum yields. Table 1 summarizes the fluorescence quantum yields, absorption maxima, molar extinction coefficients, and Stokes shifts of ethanol solutions of the metallic compounds. Figure 2 depicts steady-state spectra of ethanol solutions of three representative derivatives: **3a**, **4a**, and **4d** (respective information for the remaining compounds is provided in the Supporting Information). From Table 1, it can be seen that, in addition to the expected red shifting of the emission and absorption bands of all **4**-series compounds with respect to the corresponding derivative of the **3** series, there is a noticeable variation of the

TABLE 1: Absorption Maxima λ_{max}^{abs} (nm), Molar Extinction Coefficients ε ($M^{-1}\cdot cm^{-1}$), Stokes Shifts (cm^{-1}), and Fluorescence Quantum Yields ϕ of 3- and 4-Series Compounds

compound	λ_{max}^{abs}	$\varepsilon/10^4$	Stokes shift	ϕ^a	compound	λ_{max}^{abs}	$\varepsilon/10^4$	Stokes shift	ϕ^a
3a	445	1.4	4990	0.15	**4a**	470	1.5	4470	0.06
	316	0.8	14160			347	0.7	12010	
3b	441	1.2	3480	0.19	**4b**	467	1.3	2790	0.15
	350	1.1	9380			353	1.2	9710	
	306	1.2	13490						
3c	464	2.0	3370	0.05	**4c**	489	1.7	2590	0.10
	323	1.7	12780			357	0.7	10150	
3d	454	1.1	5390	0.04	**4d**	476	1.0	21010	0.02
	318	0.7	14810			347	0.5	12660	
3e	449	1.4	4700	0.19	**4e**	475	1.5	4270	0.08
	320	0.7	13680			346	0.7	12120	
3f	451	1.3	5530	0.05	**4f**	475	1.6	4770	0.03
	318	0.8	14810			347	0.8	12530	
3g	453	1.1	4950	0.11	**4g**	477	1.3	4300	0.06
	313	0.7	14830			349	0.6	11990	

[a] ϕ values were calculated as follows:[15,60] $\phi = \phi_R F^{(\lambda)} OD_R^{(\lambda)} \eta^2 / (F_R^{(\lambda)} OD^{(\lambda)} \eta_R^2)$, where $F^{(\lambda)}$ is the integrated area of the emission obtained by excitation at wavelength λ, $OD^{(\lambda)}$ is the optical density at the same wavelength, η is the refractive index of the solvent, and the subscript R indicates the reference molecule.

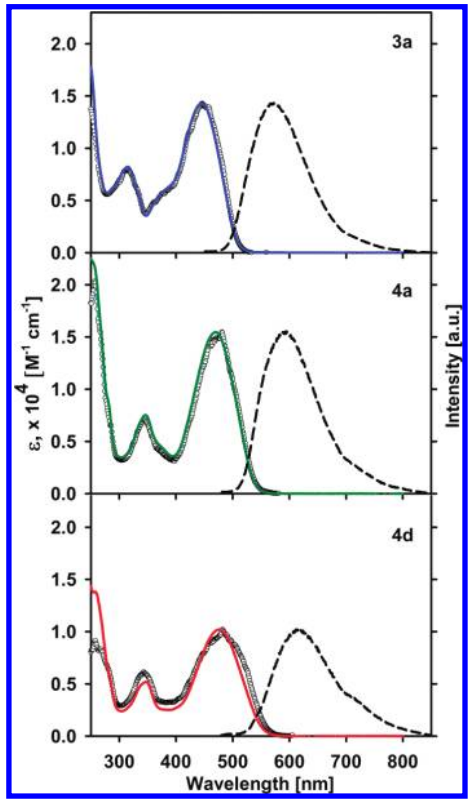

Figure 2. Molar extinction coefficient (solid colored lines) and emission (dashed lines) and excitation (circles) spectra of representative derivatives in ethanol solution. Fluorescence spectra were recorded with an excitation wavelength of 420 nm, and excitation spectra were recorded at the fluorescence maximum for each compound.

emission maxima and quantum yields along each series of compounds. Such differences can be summarized in terms of the nature and position of the substituents placed at the aniline fragment and are in full agreement with the tendency first noted on the steady-state spectra by Morisige and originally reported for beryllium, scandium, aluminum, and gallium derivatives with substituted Schiff bases:[26–28] Longer absorption and emission wavelengths are associated with the inclusion of substituents with an electron-donating capacity at the N-meta position [X = —Cl, —CH_3 and —$C(CH_3)_3$ in Scheme 1] and by electron-withdrawing substituents at the N-para position (Y = —NO_2 in our case). On the other hand, the absorption and emission bands appear at somewhat shorter wavelengths when meta-orienting groups (—NO_2) are at the N-meta position.

The existence of these substituent effects is a clear signature of a high conjugation in the system. However, as we elaborate below, for the **3** and **4** series, the aniline and salicylidene rings are not necessarily in the same plane: In the crystal phase, the structures of salicylidene-*ortho*-aminophenols (free ligands) are not far from complete planarity, showing small deviations between the salicylidene (nine atoms taken for plane calculations) and aniline moieties (eight atoms taken for plane calculations; see Scheme 1 for plane measurement explanation). From a series of reported X-ray structures,[42,49–53] depending on the nature and position of the substituents, these deviations range only from 13.44° for the *E*-OH form of **1**[49] to 2.24° when compound **1** has a nitro substituent at the O-para position in the salicylidene moiety and adopts a *Z*-NH geometry.[53] On the other hand, in the case of tin^{IV} derivatives, the size of the tin atom itself has been shown to be enough to distort planar geometries, even if a fused ring system is constructed.[16,34,37] From the X-ray structures of the diphenyl-tin^{IV} derivatives of the **3** series, it was possible to measure the following angles between planes in the organic Schiff base skeleton: 17.75° (**3a**),[54] 25.57° (**3a**),[55] 10.84° (**3c**),[35] 17.38° (**3d**),[35] 25.3° (**3e**),[35] and 19.41° (**3f**).[35] Clearly, in the tin^{IV} derivatives, the ring systems (salicylidene and aniline moieties) do not exhibit a better coplanarity than in the free Schiff bases, and therefore, the conjugation in the overall organometallic system cannot be ascribed simply to an increase in the degree of π-delocalization along the ligand skeleton, but also probably to the participation of the metal—and even the two organometallic phenyl groups—in the energy of the electronic transitions, conferring them with a charge-transfer character.

Time-Resolved Spectroscopy. As depicted in Scheme 2, the generally agreed photoinduced cycle of free Schiff bases bearing an intramolecular hydrogen bond starts with the excitation of the *E*-OH form to an S_1 (π,π^*) state that undergoes an ultrafast barrierless ESIPT process leading to a fluorescent S_1 (π,π^*) species of the *Z*-NH tautomer.[7,8] The decay of the latter isomer toward its ground state yields the so-called phototautomer, which can complete the cycle by going back to the *E*-OH form through a ground-state proton transfer (PT). In addition to internal conversion processes, another known depletion pathway that

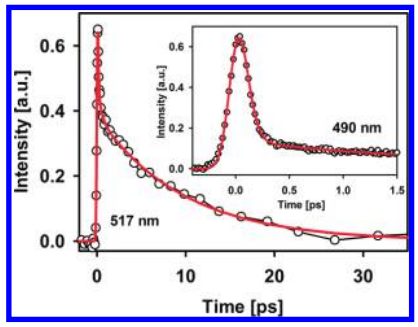

Figure 3. Fluorescence up-conversion measurements of acetonitrile solutions of **1**. The pump beam was set at 385 nm, and the emission was monitored at the wavelengths indicated in each plot. Solid thicker lines are nonlinear least-squares fits to multiexponential decay models convoluted with the instrumental response function.

partially accounts for the deactivation of the excited *Z*-NH form implies its isomerization to the S_0 state of the *E*-NH isomer (photochromic tautomer), which rapidly decays toward the more stable *Z*-NH ground state.[1–8]

Because the geometries of the *E*-OH forms of **1** and **2** force the second hydroxyl group in the aniline ring to be near the imine bond, a second intramolecular hydrogen bond can be formed. In fact, according to refs 42 and 49, the solid-state packing of the *E*-OH form of salicylidene-*ortho*-aminophenols allows the hydroxyl group from the salicylidene moiety to form hydrogen bonds with both the nitrogen and the hydroxyl group in the aniline ring. This additional hydrogen bond might alter ESIPT dynamics of **1** and **2** with respect to those of monohydroxylated Schiff bases. To gain insight into this query, we performed time-resolved up-conversion measurements of **1** and compared its excited-state dynamics with those of its extensively studied monohydroxylated analogue salicylideneaniline.[2–5,7,8] Following the procedure reported in a previous contribution,[7] we used acetonitrile as the solvent and set the excitation beam at 385 nm. For these experiments, the upconverted fluorescence was monitored at 490 and 517 nm. From the experiments with detection at 490 nm (see inset in Figure 3), we determined the time constant for the ESIPT process as 50 ± 20 fs (τ_1, from the emission decay of the locally excited *E*-OH form). Once this value was set, we adjusted the data obtained at 517 nm to a multiexponential decay (main graph in Figure 3). The other characteristic times are $\tau_2 = 370 \pm 20$ fs for the vibrational relaxation and cooling after the proton transfer has occurred (lifetime of a "hot" *Z*-NH isomer in its first electronically excited state)[1–3] and $\tau_3 = 9.6 \pm 2$ ps for the final depletion of the "cold" *Z*-NH S_1 state. The sub-100-fs decay component compares very well with the rapid lifetime of the *E*-OH isomer of salicylideneaniline in acetonitrile,[5,7] indicating the lack of effect of a second hydroxyl group in ESIPT dynamics for systems in solution.

The time-resolved emissions of ethanol solutions of **1** and **2** are shown in the main graphs of Figure 4. We included experiments in this solvent to make direct comparisons between the free bases and the diphenyl-tin^{IV} derivatives, which were studied in ethanol solution for solubility reasons. In this case, the pump beam was set at 422 nm (direct excitation of the *Z*-NH form), and the fluorescence signal was monitored at 517 nm. The fast feature ("spike" at $t = 0$) in these traces is due to self-phase modulation and Raman scattering from the flow cell, as shown by solvent-only scans taken back-to-back with the solution measurements (see Supporting Information). Fluorescence lifetimes were obtained through single-exponential fits excluding the points around $t = 0$. By this procedure, we found

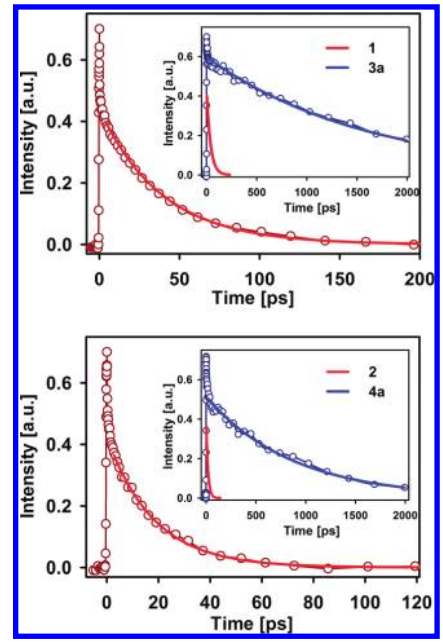

Figure 4. Fluorescence up-conversion measurements of ethanol solutions of compounds **1** (top, main), **2** (bottom, main), **3a** (top, inset), and **4a** (bottom, inset). The pump beam was set at 422 nm, and the emission was monitored at 517 nm for **1** and **2** and at 580 nm for **3a** and **4a**. Solid thicker lines are nonlinear least-squares fits to single-exponential models of the fluorescence lifetimes. For comparison purposes, fits for the **1** and **2** data are included in the insets.

time constants of 39 ± 1 ps for **1** and 17.5 ± 0.5 ps for **2**. In particular, the lifetime of **1** in ethanol is in excellent agreement with the 40 ps reported by Barbara and co-workers through the use of a Streak camera with 5-ps resolution.[2]

From the above results, it is interesting to note that the fluorescence lifetime of **2** (17.5 ps) is only about one-half that of **1** (39 ps). This suggests that the *E*−*Z* isomerization of the quinoidal form (NH) through rotation around the C_3−C_4 bond has a straightforward dependence on the motion of the aniline group. However, effects such as the barrier size, the shape of the substituents, and the specific and nonspecific (hydrodynamic friction) interactions with the solvent can sensibly affect the free-base keto-form excited-state decay.

For the participation of the Schiff base skeleton as a chromophore in the metallic derivatives **3** and **4**, we found much longer fluorescence decay times in comparison with those of the free bases. For **3a** and **4a**, the time-resolved fluorescence is depicted in the insets of Figure 4, where we have also included the fits of the decay curves of **1** and **2** for comparative purposes. Fluorescence decay curves for ethanol solutions of **3b**−**e** and **4b**−**e** are shown in Figure 5. The pump beam was set at 422 nm for **3a** and **4a** and at 390 nm for **3b**−**e** and **4b**−**e**. For all of the compounds, we monitored the upconverted fluorescence signal at 580 nm. In addition to a "long decay" in the fluorescence (see below), for all compounds, small-amplitude modulations in the traces with time constants of up to a few tens of picoseconds are present. These exponential components of the emission decay trace are due to relaxation of the system within the S_1 state (vibrational relaxation and solvation; this is further detailed in the transient absorption results). Table 2 summarizes the parameters for the emission decays for compounds **3a**−**e** and **4a**−**e**, including the first singlet excited-state lifetimes (long decay component) and the radiative rate constants. From these data, it can be seen that, except for compounds **3c** and **4c**, the excited-state lifetimes are larger for

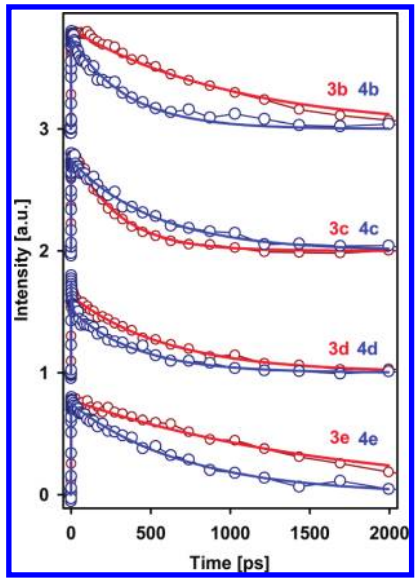

Figure 5. Fluorescence up-conversion measurements for ethanol solutions of **3b**−**e** and **4b**−**e**. The pump beam was set at 390 nm, and the emission was monitored at 580 nm. Solid thicker lines are least-squares fits to single-exponential models of the fluorescence lifetimes. All data were normalized.

TABLE 2: Up-conversion Fitting Parameters and Radiative Decay Rate Constants k_r^S of Selected Compounds[a]

compound	α_1	τ_1 (ps)	α_2	τ_2 (ns)	k_r^S (ns^{-1})[b]
3a	0.095	5.9	0.669	1.7	0.09
3b	−0.149	2.2	0.817	1.0	0.19
3c	−0.152	3.6	0.841	0.3	0.17
3d	0.158	6.5	0.632	0.6	0.07
3e	−0.323	0.7	0.777	1.7	0.11
4a	0.209	7.3	0.571	0.9	0.07
4b	−0.748	0.1	0.748	0.4	0.38
4c	−0.273	0.2	0.741	0.5	0.20
4d	0.244	6.2	0.516	0.4	0.05
4e	−	−	0.749	0.7	0.11

[a] Fitting function was set as $\alpha_1 e^{-t/\tau_1} + \alpha_2 e^{-t/\tau_2}$. [b] k_r^S values were calculated as follows:[31] $k_r^S = \phi/\tau$, where ϕ is the fluorescence quantum yield and τ is the fluorescence lifetime.

the **3** series than for the **4** series. This tendency is also followed by the fluorescence quantum yields (Table 1). The radiative decay rates (k_r^S) are higher for **4**-series compounds than for the corresponding **3**-series compounds, with the exception of compounds **3b** and **4b**. For example, we found fluorescence decay times of 1.70 ± 0.1 ns for **3a** and 0.90 ± 0.1 ns for **4a**.

Mainly, the remarkable increment in the fluorescent state lifetime of more than 50 times when the Schiff bases **1** and **2** are coordinated to a diphenyl-tin^{IV} moiety indicates that the effect of chelation with a tin^{IV} center reduces the rate of the nonradiative channels and avoids possible $E-Z$ isomerization processes, dramatically enhancing the lifetime of the first electronically excited state. It is worth noticing that this effect is not exclusive of tin, because there are some other combinations of Schiff bases with metals that are also highly fluorescent or phosphorescent.[14,20–28,30,32,33,56] In this respect, the chelating center can be seen as the molecular feature that stands for the stabilization of the S_1 state by "holding" or restricting the organic Schiff base skeleton and avoiding the loss of excitation energy through internal conversion to the ground state, or isomerization.[14,23] The variations of the decay times and quantum yields within the complexes can be rationalized by considering recent calculations of the potential energy surfaces of Schiff bases.[8]

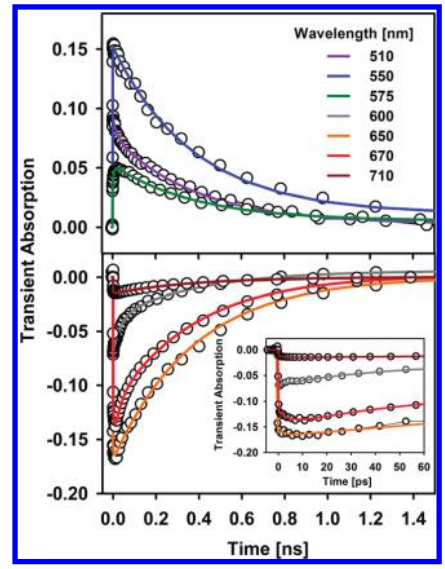

Figure 6. Transient absorption as a function of delay time for ethanol solutions of **4d**. For these experiments, the pump beam was set at 400 nm. The inset shows details of the early-time signal evolution for the stimulated emission signals.

Such studies indicate that the fluorescence quantum yield of the ligands involved in series **3** and **4** is determined at least in part, by competition between radiative decay, $E-Z$ isomerization, and direct internal conversion to the ground state. In the complexes, the proximity of the S_0 and S_1 potential energy surfaces is probably also related to the nonradiative S_1 decay channels, which, in turn, is sensitive to the extent of the aromatic system (series **3** vs **4**), as well as to the electron-withdrawing or -donating character of the substituents.

In addition to the time-resolved fluorescence experiments, we studied one of the derivatives through transient absorption measurements to ascertain the spectral regions where the different types of transient signals appear. We chose **4d** as representative of the **3** and **4** series because of its solubility and because its S_1 lifetime (~0.4 ns) allowed its excited-state dynamics to be fully observed with our experimental setup. Figure 6 shows the photoinduced absorbance change as a function of time for two spectral intervals. As can be seen, for the first case (upper graph, 510−575 nm), positive transient signals are detected, whereas for the spectral range of the lower graph (600−710 nm), the signals are due to stimulated emission (negative transient absorption signal). Except for the data at 670 nm, all transient absorption signals were fitted to a double-exponential function plus a constant term ($\alpha_1 e^{-t/\tau_1} + \alpha_2 e^{-t/\tau_2} + \alpha_3$, best-fit parameter values are included in Table 3) convoluted with the instrument response function. From a global analysis considering all single-wavelength experiments, the time constant of the slow component associated with the S_1 lifetime of the derivative was observed to be τ_2 = 380 ps, in excellent agreement with the up-conversion result. The signal at 670 nm had to be adjusted to a three-exponential function plus a constant term (two "short" τ_1 components and one slow τ_2 component set to 380 ps). The shorter time τ_1 was assigned to solvation and vibrational relaxation in the S_1 state (see below),[57,58] whereas the constant term α_3 that carries a small signal amplitude was assigned to long-lived species formed from the fluorescent state, most likely a phosphorescent triplet state. This last proposal is based on the fact that heavy main-group metals are known to strongly promote spin−orbital coupling.[20,31] In particular, phosphorescence emissions from Sn^{IV}-bearing compounds have already been reported.[20,59]

TABLE 3: Transient Absorption Fitting Parameters for Compound 4d[a]

wavelength (nm)	α_1	τ_1(ps)	α_2	α_3
475	−0.035	5.3	0.068	−0.001
510	0.015	23.5	0.074	0.003
550	−0.033	0.4	0.141	0.011
575	−0.019	6.5	0.047	0.005
600	−0.031	35.9	−0.044	0.006
650	0.015	2.9	−0.169	5×10^{-4}
670[b]	0.035, −0.034	5.3, 27.9	−0.12	0.002
710	0.002	2.7	−0.015	1×10^{-4}
760	0.002	0.9	−0.007	2×10^{-4}

[a] Fitting function was set as $\alpha_1 e^{-t/\tau_1} + \alpha_2 e^{-t/\tau_2} + \alpha_3$, where the "slow" component τ_2 was globally fitted to 380 ps. [b] For the transient stimulated emission signal at 670 nm, the signal had to be adjusted to a three-exponential function plus a constant term; therefore, two coefficients and two "short" time constants are indicated. The slow component at this wavelength was also set to 380 ps.

For the 475−575-nm region, it is clear that the signals are dominated by excited-state absorption ($S_n \leftarrow S_1$), even considering that the first absorption band of the ground state ($S_1 \leftarrow S_0$) also occurs in this region. This indicates the larger oscillator strength of the excited-state absorption transition with respect to that of the absorption from the ground state (otherwise, a negative, bleaching signal would be observed). More interestingly, for wavelengths above 600 nm, the signal is dominated by the stimulated transition. This further illustrates the potentially useful optical properties of these derivatives, where the restriction of the rapid decay channels in the organic skeleton yields highly emissive compounds that can be synthesized from very simple Schiff bases. The short-time signal evolution (see Figure 6, inset) consists of small-amplitude changes in the transient signals that reflect the time scale on which the vibrational relaxation in the first excited singlet potential energy surface takes place (up to a few tens of picoseconds; see τ_1 values in Table 3). These observations indicate that, although the molecule reaches its lowest vibrational energy in the fluorescent state, the interaction with the metal center (bischelation) restricts the ligand from exploring the potential energy surface in regions where the molecules can undergo deactivation (internal conversion to the ground state or isomerization) as in the case of the free ligands.

Two-Photon Absorption Cross Sections (TPACSs). Because of their much improved fluorescent character and the current interest in developing metal coordination compounds with high two-photon absorption abilities and other nonlinear optical properties,[16–19,56] we measured the TPACSs of the **3** and **4** series of compounds, taking advantage of their emissive nature. TPACSs (∂) were calculated as follows[46–48]

$$\partial^{(\lambda)} = \partial_R^{(\lambda)} \frac{F^{(2,\lambda)} C_R \phi_R^{(2)} \eta_R}{F_R^{(2,\lambda)} C \phi^{(2)} \eta}$$

where $F^{(2,\lambda)}$ is the integrated area of the emission bands obtained by two-photon excitation at the pump wavelength λ, C is the concentration (in mol L^{-1}), $\phi^{(2)}$ is the two-photon excitation fluorescence quantum yield, and the subscript R stands for the respective values of the reference molecule (rhodamine B in methanol). Because of its rapid relaxation, the two-photon excitation fluorescence (TPEF) comes from the lowest vibrational level of the S_1 excited state, so the one-photon and two-photon excitation fluorescence spectra are essentially identical and $\phi^{(2)}$ is taken to be equal to ϕ.[60] Values for δ_R were taken as reported elsewhere.[44]

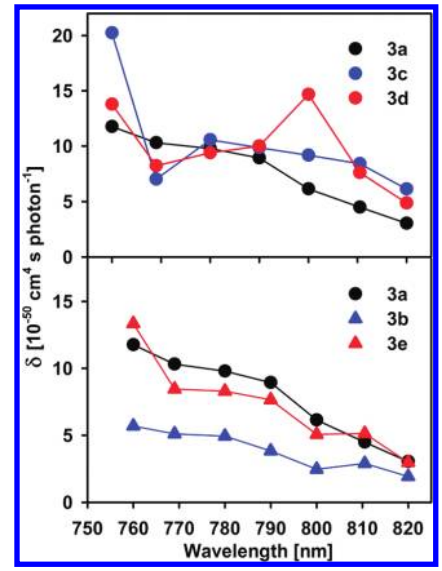

Figure 7. Two-photon absorption cross sections (TPACSs) for representative **3**-series compounds. To allow for easier visualization of the data, the results for derivatives with enhanced TPACS values with respect to **3a** are plotted in the upper graph.

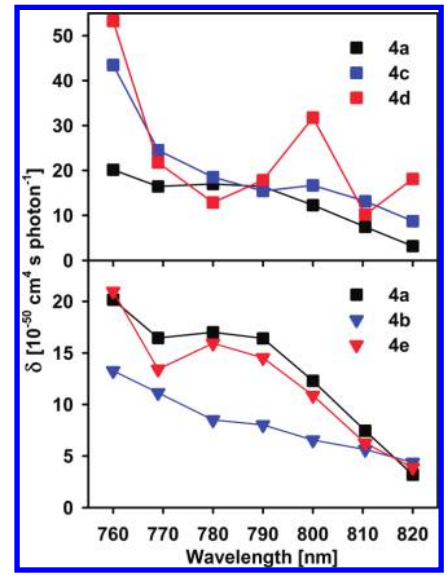

Figure 8. Two-photon absorption cross sections (TPACSs) for representative **4**-series compounds. To allow for easier visualization of the data, the results for derivatives with enhanced TPACS values with respect to **4a** are plotted in the upper graph.

In Figures 7 and 8, we have plotted the TPACSs of representative derivatives of the **3** and **4** series, respectively. The plots in each figure are divided into two groups to allow an easier visual analysis of the data: In both figures, the upper graphs display the TPACSs of those compounds with improved values compared to **3a** and **4a**, whereas the bottom plots present the results of those compounds that exhibit smaller values. Results for the remaining compounds are provided as Supporting Information. It can be clearly seen that, in both kinds of diphenyl-tin^{IV} derivatives, whether they have a Schiff base ligand with a salicylidene (**3** series) or a naphthalydene (**4** series) moiety, the same trend is followed: TPACSs are enhanced by groups that have an electron-donating capability placed at the N-meta position and electron-withdrawing groups at N-para position.

Compounds **3** and **4** can be seen as a cyclic π-donor−acceptor system ($-\pi-$D$-$A$-\pi-$), where the π-donor group is the nitrogen and the π-acceptor is the organometallic group, both bridged by the aromatic rings of the aniline and the salicylidene (**3**) or naphthalidene (**4**) groups. It has been found that high TPACS values are associated with the inclusion of several electron-donor and -acceptor groups and to an extensive π-delocalization.[18,19,47,61] This is in agreement with the fact that TPACS values of compounds with a naphthalene moiety (**4**), which includes more π-conjugation, are higher than those of their analogues with a salicylidene moiety (**3**). Further evidence of the latter is found in the substituents' effects, because the trends that were found to increase TPACS values were also found to cause a red shift of both absorption and emission bands (see Steady-State Spectroscopy section). Although clear, the differences in TPACSs caused by different substituents in the aniline ring are not extreme, and we explain this by the fact that the substituents are in one of the π-bridges and, as a result, their electron-withdrawing and electron-donating capabilities affect both the D and A groups in the cyclic $-\pi-$D$-$A$-\pi-$ pattern.

TPACS values of **3** and **4** are probably not high enough for their direct use in applications based on nonlinear optic processes. However, the recently reported high two-photon absorbers based on other metallic compounds with Schiff bases as ligands[18,19,62] suggest that TPACSs can be improved by orders of magnitude by changing the extension and conjugation of the organic skeleton, as well as the nature of the chelating moiety. The identification of the substituent effects on the two-photon absorption ability of these derivatives presented herein consolidates an interesting case study for the highly pursued design of compounds with high two-photon absorption ability. Here, it is worth emphasizing that their highly emissive nature makes it possible to measure these nonlinear optical properties through their fluorescence excitation spectra.

Conclusions

We have synthesized and performed a systematic study of the photophysics of 14 diphenyl-tin^{IV} derivatives with Schiff bases in ethanol solution and compared them with those of the free Schiff bases **1** and **2**. We found an important enhancement of fluorescence when the Schiff base framework is used as a chelating ligand. Regarding time-resolved up-conversion measurements, we found that the fluorescence lifetimes of the diorgano-tin^{IV} derivatives **3a** and **4a** are more than 50 times larger than those of the free Schiff bases **1** and **2**. Because this chelation-induced enhancement of fluorescence has already been reported for several other Schiff base derivatives,[14,20–28,30,32,33,56] we attribute the enhanced fluorescent character and the longer decay times of such molecules to an effect of chelation, where the metallic center acts as a molecular feature that avoids the loss of excitation energy by not allowing the organic skeleton to fully explore its potential energy surface.

Taking advantage of their improved emissive character, we determined the TPACSs of the **3**- and **4**-series compounds by directly measuring their TPEF spectra. Moreover, we performed transient absorption experiments that allowed us to assess the wide wavelength range (600−710 nm) where this type of derivative is susceptible to produce stimulated emission. Their enhanced fluorescent character and large stimulated emission interval, along with their specific synthetic versatility,[16,34–36,42,43,63] as well as the possibility of tuning their photophysical features by changing the length of the organic skeleton and even the nature of the chelated center,[14] confirm the studied metallic derivatives as important models to take into account for the design of new molecular entities and materials with highly nonlinear optical applications and the construction of light-emitting devices.

Acknowledgment. We are thankful to Professor Ahmed H. Zewail and the California Institute of Technology for the donation of equipment used in this study. For financial support, we thank Consejo Nacional de Ciencia y Tecnología (CONACyT, Grant 79494) and Universidad Nacional Autónoma de México (PAPIIT, Grant IN212907). We also thank M.Sc. Nieves Zavala Segovia and M.Sc. Luis Velasco Ibarra for the acquisition of the NMR and mass spectra of the compounds of this study.

Supporting Information Available: Steady-state spectra of compounds **3b**−**g**, **4b**, **4c**, and **4e**−**g**; single-wavelength fluorescence up-conversion traces for back-to-back experiments of pure ethanol and ethanol solutions of **1** and **2** that show the presence of a fast feature at early times; and two-photon absorption cross section information for compounds **3a**, **3f**, **3g**, **4a**, **4f**, and **4g**. This material is available free of charge via the Internet at http://pubs.acs.org.

References and Notes

(1) Barbara, P. F.; Brus, L. E.; Rentzepis, P. M. *J. Am. Chem. Soc.* **1980**, *102*, 5631.
(2) Barbara, P. F.; Rentzepis, P. M.; Brus, L. E. *J. Am. Chem. Soc.* **1980**, *102*, 2786.
(3) Mitra, S.; Tamai, N. *Phys. Chem. Chem. Phys.* **2003**, *5*, 4647.
(4) Zgierski, M. Z.; Grabowska, A. *J. Chem. Phys.* **2000**, *112*, 6329.
(5) Ziółek, M.; Kubicki, J.; Maciejewski, A.; Naskręcki, R.; Grabowska, A. *Phys. Chem. Chem. Phys.* **2004**, *6*, 4682.
(6) Ziółek, M.; Burdziński, G.; Filipczak, K.; Karolczak, J. *Phys. Chem. Chem. Phys.* **2008**, *10*, 1304.
(7) Rodríguez-Córdoba, W.; Zugazagoitia, J. S.; Collado-Fregoso, E.; Peon, J. *J. Phys. Chem. A* **2007**, *111*, 6241.
(8) Ortiz-Sánchez, J. M.; Gelabert, R.; Moreno, M.; Lluch, J. M. *J. Chem. Phys.* **2008**, *129*, 214308.
(9) Dziembowska, T.; Jagodzińska, E.; Rozwadowski, Z.; Kotfica, M. *J. Mol. Struct.* **2001**, *598*, 229.
(10) Sahoo, S. K.; Bera, R. K.; Baral, M.; Kanungo, B. K. *J. Photochem. Photobiol. A* **2007**, *188*, 298.
(11) Ohshima, A.; Momotake, A.; Arai, T. *J. Photochem. Photobiol. A* **2004**, *162*, 473.
(12) Antonov, L.; Fabian, W. M. F.; Nedeltcheva, D.; Kamounah, F. S. *J. Chem. Soc., Perkin Trans. 2* **2000**, 1173.
(13) Joshi, H.; Kamounah, F. S.; Gooijer, C.; van der Zwan, G.; Antonov, L. *J. Photochem. Photobiol. A* **2002**, *152*, 183.
(14) Freeman, D. C.; White, C. E. *J. Am. Chem. Soc.* **1956**, *78*, 2678.
(15) Zhao, L.; Hou, Q.; Sui, D.; Wang, Y.; Jiang, S. *Spectrochim. Acta A* **2007**, *67*, 1120.
(16) Reyes, H.; García, C.; Farfán, N.; Santillan, R.; Lacroix, P. G.; Lepetit, C.; Nakatani, K. *J. Organomet. Chem.* **2004**, *689*, 2303.
(17) Li, S.-L.; Wu, J.-Y.; Tian, Y.-P.; Tang, Y.-W.; Jiang, M.-H.; Fun, H. K.; Chantrapromma, S. *Opt. Mater.* **2006**, *28*, 897.
(18) Das, S.; Nag, A.; Goswami, D.; Bharadwaj, P. K. *J. Am. Chem. Soc.* **2006**, *128*, 402.
(19) Ye, Z.; De Boni, L.; Neves, U. M.; Mendonça, C. R.; Bu, X. R. *Tetrahedron Lett.* **2009**, *50*, 1371.
(20) Jia, W.-L.; Liu, Q.-D.; Wang, R.; Wang, S. *Organometallics* **2003**, *22*, 4070.
(21) Qiao, J.; Wang, L. D.; Duan, L.; Li, Y.; Zhang, D. Q.; Qiu, Y. *Inorg. Chem.* **2004**, *43*, 5096.
(22) Qiao, J.; Wang, L. D.; Xie, J. F.; Lei, G. T.; Wu, G. S.; Qiu, Y. *Chem. Commun.* **2005**, 4560.
(23) Kagkelari, A.; Bekiari, V.; Stathatos, E.; Papaefstathiou, G. S.; Raptopoulou, C. P.; Zafiropoulos, T. F.; Lianos, P. *J. Lumin.* **2009**, *129*, 578.
(24) Hou, Q.; Zhao, L.; Zhang, H.; Wang, Y.; Jiang, S. *J. Lumin.* **2007**, *126*, 447.
(25) Dagnall, R. M.; Smith, R.; West, T. S. *Talanta* **1966**, *13*, 609.
(26) Morisige, K. *Anal. Chim. Acta* **1974**, *72*, 295.
(27) Morisige, K. *Anal. Chim. Acta* **1974**, *73*, 245.
(28) Morisige, K. *J. Inorg. Nucl. Chem.* **1978**, *40*, 843.

(29) Bhardwaj, V. K.; Pannu, A. P. S.; Singh, N.; Hundal, M. S.; Hundal, G. *Tetrahedron* **2008**, *64*, 5384.
(30) Yoshino, J.; Kano, N.; Kawashima, T. *J. Org. Chem.* **2009**, *74*, 7496.
(31) Klessinger, M.; Michl, J. *Excited States and Photochemistry of Organic Molecules*; VCH: New York, 1995.
(32) Takano, K.; Shibahara, T. *Chem. Lett.* **2008**, *37*, 70.
(33) Yoshino, J.; Kano, N.; Kawashima, T. *Chem. Commun.* **2007**, 559.
(34) Barba, V.; Vega, E.; Luna, R.; Höpfl, H.; Beltrán, H. I.; Zamudio-Rivera, L. S. *J. Organomet. Chem.* **2007**, *692*, 731.
(35) Beltrán, H. I.; Damian-Zea, C.; Hernández-Ortega, S.; Nieto-Camacho, A.; Ramírez-Apan, M. T. *J. Inorg. Biochem.* **2007**, *101*, 1070.
(36) Zamudio-Rivera, L. S.; George-Tellez, R.; López-Mendoza, G.; Morales-Pacheco, A.; Flores, E.; Höpfl, H.; Barba, V.; Fernández, F. J.; Cabirol, N.; Beltrán, H. I. *Inorg. Chem.* **2005**, *44*, 5370.
(37) Farfán, N.; Mancilla, T.; Santillan, R.; Gutiérrez, A.; Zamudio-Rivera, L. S.; Beltrán, H. I. *J. Organomet. Chem.* **2004**, *689*, 3481.
(38) Luna-García, R.; Damián-Murillo, B. M.; Barba, V.; Höpfl, H.; Beltrán, H. I.; Zamudio-Rivera, L. S. *Chem. Commun.* **2005**, 5527.
(39) Hernández-Ahuactzi, I. F.; Cruz-Huerta, J.; Barba, V.; Höpfl, H.; Zamudio-Rivera, L. S.; Beltrán, H. I. *Eur. J. Inorg. Chem.* **2008**, *2008*, 1200.
(40) Beltrán, H. I.; Zamudio-Rivera, L. S.; Mancilla, T.; Santillan, R.; Farfán, N. *Chem.—Eur. J.* **2003**, *9*, 2291.
(41) Barba, V.; Vega, E.; Höpfl, H.; Zamudio-Rivera, L. S.; Domínguez-Aguilar, M. A.; George-Tellez, R.; Godínez-Salomon, F.; Hallen-Lopez, J. M.; Beltran, H. I. *Eur. J. Inorg. Chem.* **2007**, *2007*, 927.
(42) Labisbal, E.; Rodríguez, L.; Vizoso, A.; Alonso, M.; Romeros, J.; García-Vázquez, J.-A.; Sousa-Pedrares, A.; Sousa, A. *Z. Anorg. Allg. Chem.* **2005**, *631*, 2107.
(43) Pettinari, C.; Marchetti, F.; Pettinari, R.; Martini, D.; Drozdov, A.; Troyanov, S. *Inorg. Chim. Acta* **2001**, *325*, 103.
(44) Xu, C.; Webb, W. W. *J. Opt. Soc. Am. B* **1996**, *13*, 481.
(45) Zugazagoitia, J. S.; Collado-Fregoso, E.; Plaza-Medina, E. F.; Peon, J. *J. Phys. Chem. A* **2009**, *113*, 805.
(46) Albota, M. A.; Xu, C.; Webb, W. W. *Appl. Opt.* **1998**, *37*, 7352.
(47) Shao, P.; Huang, B.; Chen, L.; Liu, Z. L.; Qin, J.; Gong, H.; Ding, S.; Wang, Q. *J. Mater. Chem.* **2005**, *15*, 4502.
(48) Oulianov, D. A.; Tomov, I. V.; Dvornikov, A. S.; Rentzepis, P. M. *Opt. Commun.* **2001**, *191*, 235.
(49) Elerman, Y.; Elmali, A.; Atakol, O.; Svodoba, I. *Acta Crystallogr. C: Cryst. Struct. Commun.* **1995**, *C51*, 2344.
(50) Mukherjee, A. K.; De, R. L.; Banerjee, I.; Samanta, C.; Nayak, N. P. *Acta Crystallogr. C: Cryst. Struct. Commun.* **1999**, *C55*, 407.
(51) Ondráček, J.; Kováøová, Z.; Maixner, J.; Jursik, F. *Acta Crystallogr. C: Cryst. Struct. Commun.* **1993**, *C49*, 1948.
(52) Elmali, A.; Kabak, M.; Kavlakoglu, E.; Elerman, Y.; Durlu, T. N. *J. Mol. Struct.* **1999**, *510*, 207.
(53) Böhme, U.; Fels, S. *Acta Crystallogr. E: Struct. Rep. Online* **2008**, *E64*, o178.
(54) Preut, H.; Huber, F.; Barbieri, R.; Bertanzzi, N. *Z. Anorg. Allg. Chem.* **1976**, *423*, 75.
(55) Diamantis, A. A.; Gulbis, J. M.; Manikas, M.; Tiekink, E. R. T. *Phosphorus, Sulfur Silicon Relat. Elem.* **1999**, *150−151*, 251.
(56) Tian, Y.-P.; Zhang, M.-L.; Hu, Z.-J.; Hu, H.-M.; Wu, J.-Y.; Zhang, X.-J.; Zhang, S.-Y. *Transition Met. Chem.* **2005**, *30*, 778.
(57) Tan, X.; Gustafson, T. L.; Lefumeux, C.; Burdzinski, G.; Buntinx, G.; Poizat, O. *J. Phys. Chem. A* **2002**, *106*, 3593.
(58) Sukowski, U.; Seilmeier, A.; Elsaesser, T.; Fischer, S. F. *J. Chem. Phys.* **1990**, *93*, 4094.
(59) Wang, L.-S.; Sheng, T.-L.; Wang, X.; Chen, D.-B.; Hu, S.-M.; Fu, R.-B.; Xiang, S.-C.; Wu, X.-T. *Inorg. Chem.* **2008**, *47*, 4054.
(60) Fischer, A.; Cremer, C.; Stelzer, E. H. K. *Appl. Opt.* **1995**, *34*, 1989.
(61) Albota, M.; Beljonne, D.; Brédas, J. L.; Ehrlich, J. E.; Fu, J. Y.; Heikal, A. A.; Hess, S. E.; Kogej, T.; Levin, M. D.; Marder, S. R.; McCord-Maughon, D.; Perry, J. W.; Röckel, H.; Rumi, M.; Subramaniam, C.; Webb, W. W.; Wu, X. L.; Xu, C. *Science* **1998**, *281*, 1653.
(62) Tian, L.; Hu, Z.; Shi, P.; Zhou, H.; Wu, J.; Tian, Y.; Zhou, Y.; Tao, X.; Jiang, M. *J. Lumin.* **2007**, *127*, 423.
(63) Öztaş, N. A.; Yenişehirli, G.; Ancın, N.; Öztaş, S. G.; Özcan, Y.; Ide, S. *Spectrochim. Acta A* **2009**, *72*, 929.

JP904784B